Astron. Astrophys. 353, 575–582 (2000)

ASTRONOMY AND ASTROPHYSICS

BeppoSAX spectroscopy of the Hercules X-1 short-on state

T. Oosterbroek[1], **A.N. Parmar**[1], **D. Dal Fiume**[2], **M. Orlandini**[2], **A. Santangelo**[3], **S. Del Sordo**[3], **and A. Segreto**[3]

[1] Astrophysics Division, Space Science Department of ESA, ESTEC, P.O. Box 299, 2200 AG Noordwijk, The Netherlands
[2] Istituto TESRE, CNR, via Gobetti 101, 40129 Bologna, Italy
[3] IFCAI, CNR, via La Malfa 153, 90146 Palermo, Italy

Received 15 July 1999 / Accepted 11 October 1999

Abstract. We present results of a 5.7 day duration BeppoSAX observation of the short-on state of Her X-1 and a short observation during the decline of the preceding main-on state. The 0.1–10 keV spectra can be fit with a power-law and blackbody model together with Fe emission features at 1.0 keV and 6.5 keV. During the later stages of the short-on state there are long intervals when the absorption is $\gtrsim 5 \times 10^{22}$ atom cm^{-2}. These intervals become longer and occur $\sim$0.3 day earlier in each orbital cycle as the short-on state progresses. During the intervals of high absorption the 0.1 keV blackbody is still clearly detected. This may indicate the presence of separate scattered and absorbed spectral components, although other explanations such as partial covering or a partially ionized absorber cannot be excluded. During the rest of the short-on state the ratio of flux in the blackbody compared to the power-law is consistent with that in the main-on state. This supports the view that much of the 35 day modulation is caused by an energy independent process, such as electron scattering. The discovery of strong absorption late in the short-on state is consistent with the predictions of the warped disk model (Petterson 1977, see also Schandl & Meyer 1994) where the end of the short-on state is caused by the accretion disk moving into the line of sight to the neutron star. The pulse phase difference between the blackbody and the power-law maxima is $250 \pm 20^\circ$ in both observations (separated by 0.43 of a 35 day cycle). This constant phase difference is consistent with the blackbody originating at the inner edge of a precessing accretion disk.

Key words: accretion, accretion disks – stars: individual: Her X-1 – stars: neutron – X-rays: stars

1. Introduction

Her X-1 is an eclipsing X-ray pulsar with a pulse period of 1.24 s and an orbital period of 1.70 days (Tananbaum et al. 1972; Giacconi et al. 1973). The source exhibits a 35 day X-ray intensity cycle consisting of a $\sim$10 day duration main on-state between $\Phi_{35} = 0.0 - 0.31$ (using the ephemeris of Scott & Leahy (1999) where $\Phi_{35} = 0.0$ is defined as the turn-on to the main-on state) and a fainter $\sim$5 day duration secondary, or short, on-state between Φ_{35} = 0.57–0.79. At other Φ_{35} Her X-1 is still visible as a low-level X-ray source (Jones & Forman 1976). This modulation has been ascribed to a tilted precessing accretion disk (Gerend & Boynton 1976) and an accretion disk corona Schandl & Meyer (1994) that periodically obscure the line of sight to the neutron star. In the warped disk model of Schandl & Meyer (1994) and Schandl (1996), the onset of the main-on state is caused by the edge of the accretion disk moving out of the line of sight to the neutron star and the end of the main-on state is caused by the corona crossing the line of sight. The onset of the main-on state is associated with an increase in photoelectric absorption by cold material, while no such increase is seen during its more gradual decay (e.g., Becker et al. 1977; Parmar et al. 1980). In addition, a regular pattern of narrow X-ray intensity dips are observed which repeat every 1.65 days. These are probably caused by obscuration from cold material in the outer regions of the accretion disk (Crosa & Boynton 1980)

The broad-band on-state X-ray spectrum of Her X-1 is known to be complex and consists of at least the following components: (1) a power-law with a photon index, α, of $\sim$0.9 in the energy range 2–20 keV. (2) Cyclotron absorption (Trümper et al. 1978; Mihara et al. 1990) at energies $\gtrsim$20 keV. (3) A broad Fe emission feature near 6.4 keV (Pravdo et al. 1977; Choi et al. 1994). (4) A blackbody with a temperature, kT, of $\sim$0.1 keV (Shulman et al. 1975; Catura & Acton 1975; McCray et al. 1982; Mavromatakis 1993; Vrtilek et al. 1994; Choi et al. 1997; Oosterbroek et al. 1997, hereafter O97) and (5) a broad emission feature between 0.8–1.4 keV, which is probably unresolved Fe L shell emission (McCray et al. 1982; Mihara & Soong 1994; O97).

Pulse-phase spectroscopy using the *Einstein* Objective Grating (OGS) and Solid State Spectrometers (SSS) in the energy range 0.15–4.5 keV by McCray et al. (1982) revealed that the maximum intensities of the blackbody and power-law components are shifted by 240° during the main-on state. It is likely that the blackbody component results from hard X-rays that are reprocessed in the illuminated inner regions of the accretion disk. McCray et al. (1982) note that the phase of maximum intensity of the unresolved 0.8–1.4 keV feature appears coincident with that of the blackbody. The pulse-phase dependence of the blackbody component was investigated with better quality data

Send offprint requests to: T. Oosterbroek (toosterb@astro. estec.esa.nl)

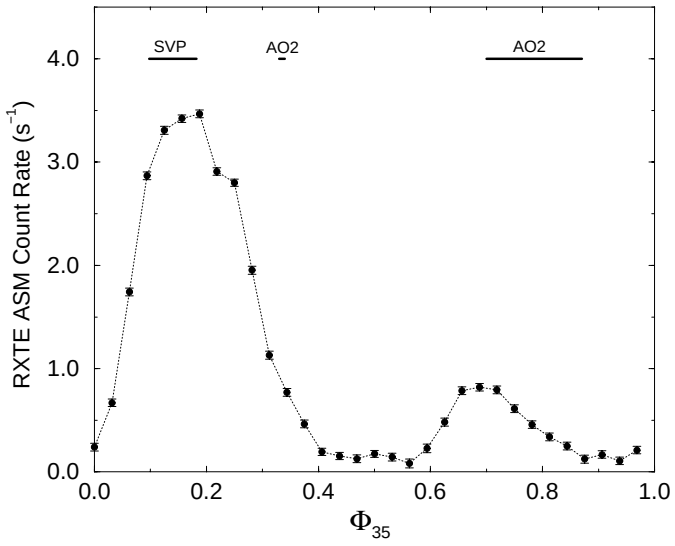

Fig. 1. The mean 35 day intensity cycle of Her X-1 measured by the RXTE ASM. The phases, Φ_{35}, of the Science Verification Phase (SVP) and AO2 main- and short-on state observations (AO2) are indicated

by O97 who confirmed the above phase-difference, and established that the Fe-L line and the blackbody exhibit a similar phase-dependent behavior during the main-on state.

In this *paper* we report on a BeppoSAX observation designed to investigate the nature of the short-on state modulation. An additional short observation was performed during the declining phase of the preceding main-on state for comparison purposes. We concentrate on the 0.1–10 keV spectrum of Her X-1, which contains all the continuum and reprocessed components.

2. Observations

Results from the Low-Energy Concentrator Spectrometer (LECS; 0.1–10 keV; Parmar et al. 1997), and the Medium-Energy Concentrator Spectrometer (MECS; 1.8–10 keV; Boella et al. 1997) on-board BeppoSAX are presented. The MECS consists of two grazing incidence telescopes with imaging gas scintillation proportional counters in their focal planes. The LECS uses an identical concentrator system as the MECS, but utilizes an ultra-thin entrance window and a driftless configuration to extend the low-energy response to 0.1 keV.

The main-on state observation was performed during the trailing edge of the on-state, significantly later in Φ_{35} than the observation reported in O97. The 5.7 day duration short-on state observation covered most of the short-on state (and possibly some low-state at the end), but did not include the turn-on. The main-on state observation started at 1998 June 27 08:34 and lasted until June 28 02:56 (UTC). The short-on state observation lasted from 1998 July 9 20:38 until July 15 15:13 (UTC). Fig. 1 illustrates the Φ_{35} coverage of the three BeppoSAX observations of Her X-1 discussed here. The dashed line shows the mean 35 day 2–12 keV intensity profile obtained by folding the Rossi X-ray Timing Explorer (RXTE) All-sky Monitor (ASM) data obtained between 1996 February 20 and 1999 February 24 over the best-fit period of 34.75 days. The difference in Φ_{35} between the mid-times of the two observations discussed here is 0.43.

LECS and MECS data were extracted centered on the Her X-1 position using radii of $8'$ and $4'$, respectively. Good data were selected from intervals when the minimum elevation angle above the Earth's limb was $>5^\circ$ ($>4^\circ$ for the LECS) and when the instrument configuration was nominal using the SAXDAS 1.8.0 data analysis package. Spectral analysis was performed with the response matrix from the 1997 September release of SAXDAS for the MECS and a response matrix appropriate for the source position in the LECS field of view using LEMAT 3.5.6. The total main-on state exposures are 18 ks and 25 ks for the LECS and MECS, respectively. The total short-on state exposure times are 125 ks and 165 ks for the LECS and MECS, respectively.

3. Analysis and results

3.1. X-ray lightcurve

The 0.1–1.0 keV LECS and 1.8–10 keV MECS lightcurves of both observations are shown in Fig. 2 together with the hardness ratios (LECS counts between 4–10 keV divided by those between 0.1–1.0 keV). The ordinate extrema are the same for both on-states, but the time axes have different scales, with the main-on state plots expanded by about a factor of 2. Eclipse intervals based on the orbital ephemeris of Deeter et al. (1991) and assuming an on-state eclipse duration of 5.5 hour are indicated.

A number of new and interesting features are evident. Soon after the start of the main-on state observation there is an interval of dipping activity (the modulation is much stronger in the LECS than the MECS, consistent with the known energy dependence of dipping), followed by a dip-free interval and a longer interval of deep dipping at the end of the observation. The short-on state observation covers parts of 4 orbital cycles and includes 3 eclipse intervals. Both the LECS and the MECS show a gradual reduction in count rate, with this effect being more pronounced in the LECS, such that the fourth orbital cycle appears to be absent, whereas a small modulation is still visible in the MECS. Superposed on this decay are the eclipses and what is normally taken to be dipping activity. However, this appears to be present for up to 20 hrs during each orbital cycle, whereas the main-on state dip duration is usually 5–10 hr (see e.g., Reynolds & Parmar 1995; Scott & Leahy 1999). During the first three orbital cycles, the centroid of the emission occurs at successively earlier orbital phases, while for the fourth orbital cycle no strong variation within the cycle is observed. This is also seen in the hardness ratio plot which shows intervals of increased hardness (consistent with increased absorption) that occur progressively earlier in each of the first 3 (and possibly the fourth) orbital cycles. The peaks of the MECS centroids and the increases in LECS hardness ratio seen in Fig. 2 are separated by an average of $\sim$1.4 days. This means that the intervals of strong absorption march back by $\sim$7 hr each orbital cycle. This rapid marching back is in strong contrast to the main-on state dips which have a period only 0.5 hr less than the orbital one (Scott & Leahy 1999). There may also be a narrow intensity dip in the

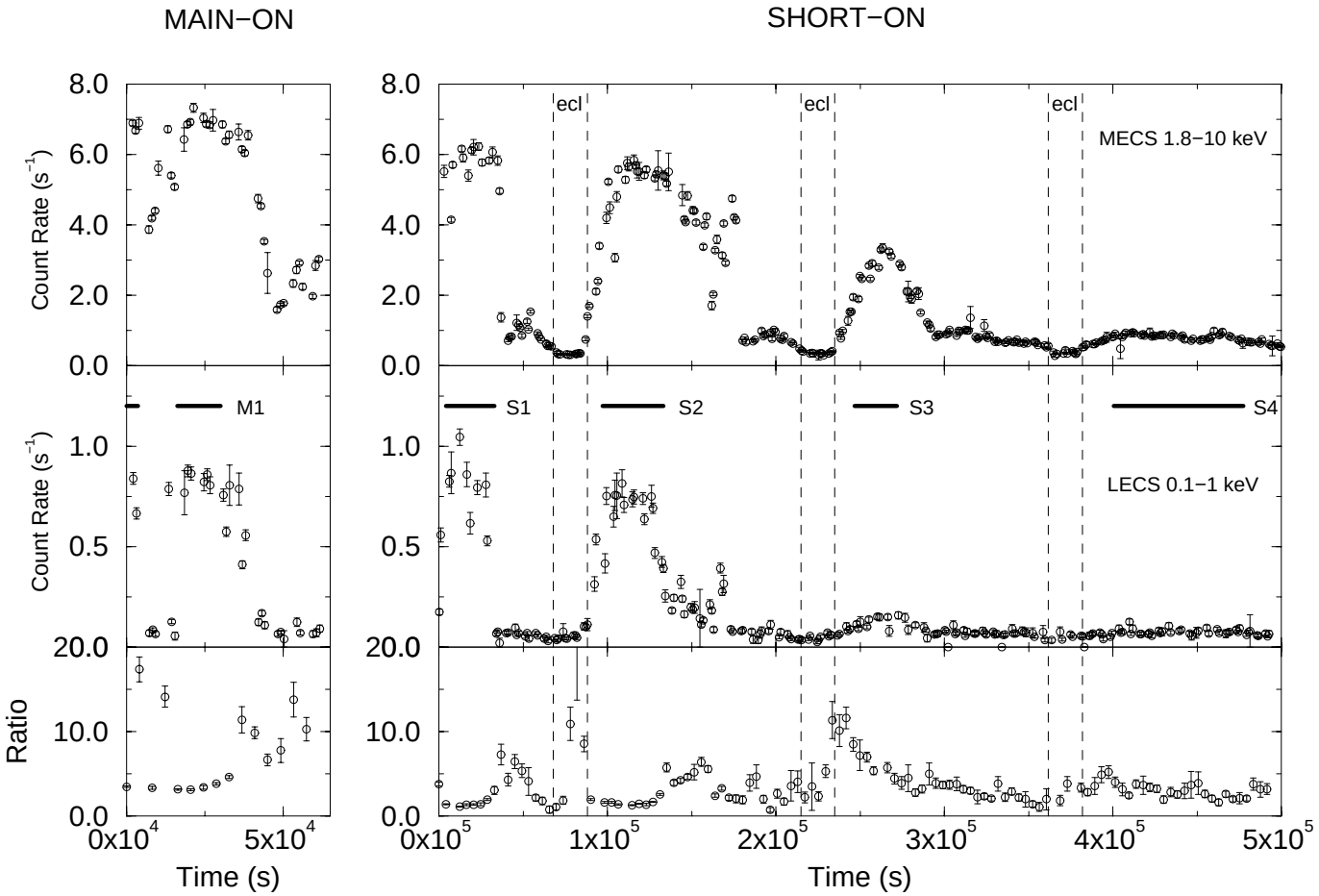

Fig. 2. MECS 1.8–10 keV (upper panels) and LECS 0.1–1.0 keV (middle panels) lightcurves obtained during the main- (left) and short-on state (right) observations with a binning of 1024 s. Note the different temporal scales. The predicted eclipse times and durations, using the ephemeris of Deeter et al. (1991), are indicated with dashed lines. The intervals M1 and S1 to S4, used to extract continuum spectra, are indicated by horizontal bars (see Sect. 3.2). Times are seconds since the start of each observation. The lower panels show the LECS hardness ratio (4.0–10 keV/0.1–1.0 keV) plotted with a binning of 4096 s

MECS lightcurve, similar to those seen in the on-state, towards the end of the second cycle of the short-on state.

3.2. X-ray spectrum

In order to study the spectral evolution during the parts of the 35 day cycle observed here, 5 phase averaged spectra were extracted. The selected intervals are indicated in Fig. 2 and are labelled as M1 and S1 to S4. Interval M1 covers a dip-free part of the main-on state, while S1 and S2 cover the peaks of the first two short-on orbital cycles and have a similar overall intensity to M1. Interval S3 covers part of the third short-on orbital cycle, where the LECS intensity is severely reduced, while S4 covers most of the final short-on cycle, which may also include low-state emission.

The spectra were rebinned to oversample the full width half maximum (FWHM) of the energy resolution by a factor 3 and to have additionally a minimum of 20 counts per bin to allow use of the χ^2 statistic. Additionally a 2% systematic error was added to the uncertainties. Events were selected in the energy ranges 0.1–4.0 keV (LECS) and 1.8–10 keV (MECS) where the instrument responses are well determined and sufficient counts obtained. The photoelectric absorption cross sections of Morisson & McCammon (1983) and the solar abundances of Anders & Grevesse (1989) are used throughout. A factor was included in the spectral fitting to allow for normalization uncertainties between the instruments. This was constrained to be within the usual range of 0.8–1.0 (LECS/MECS) during all fitting.

Initially, all 5 spectra were fit with the absorbed power-law and blackbody continuum together with 2 broad Gaussian emission features at $\sim$1 keV and $\sim$6.4 keV as used by O97. The ASCA Solid-State Imaging Spectrometer (SIS) results of Mihara & Soong (1994) indicate that the $\sim$1 keV feature may be better modeled as two narrow lines at at 0.91 keV and 1.06 keV, at least in the low-state. Since the full-width half maximum (FWHM) energy resolution of the LECS is 0.2 keV at 1 keV, these features are not well resolved in the LECS and so the broad feature was replaced by two narrow lines with the energies fixed at the above values in all subsequent fits. We refer to this as the "standard" model. The fit results presented in Table 1 indicate

Table 1. Spectral fit parameters and 90% confidence uncertainties for the phase-averaged spectral fits. The spectra have been fit with the "standard" model. The energies of the narrow Fe-L lines were fixed at the best-fit ASCA values in Mihara & Soong (1994). The equivalent blackbody radius assumes a distance of 6.6 kpc (Reynolds et al. 1997). The (0.1–10 keV) intensity is for all spectral components

Parameter	Spectrum				
	M1	S1	S2	S3	S4
LECS/MECS exposure (ks)	6.6/8.6	4.5/7.3	7.4/10.9	7.6/9.7	19.8/26.6
α	$0.753\pm^{0.017}_{0.012}$	$0.787\pm^{0.021}_{0.011}$	$0.802\pm^{0.020}_{0.009}$	0.53	0.50 ± 0.03
Blackbody kT (keV)	$0.097\pm^{0.006}_{0.002}$	$0.094\pm^{0.004}_{0.003}$	$0.094\pm^{0.002}_{0.005}$	0.12	0.101 ± 0.008
Equiv. BB radius (km)	215 ± 16	209 ± 13	202 ± 10	262	$67\pm^{59}_{67}$
N_H ($\times 10^{19}$ atom cm^{-2})	$0.15\pm^{0.10}_{0.15}$	$0.19\pm^{0.13}_{0.11}$	0.22 ± 0.07	750	<0.6
Fe-L 0.91 keV EW (eV)	100 ± 30	$95\pm^{30}_{20}$	70 ± 30	0.0	$4\pm^{41}_{4}$
Fe-L 1.06 keV EW (eV)	65 ± 30	60 ± 30	40 ± 40	0.0	125 ± 50
Fe-K line energy (keV)	$6.445\pm^{0.13}_{0.03}$	6.50 ± 0.07	6.52 ± 0.05	6.156	6.55 ± 0.05
Fe-K line FWHM (keV)	$0.83\pm^{0.26}_{0.13}$	$0.92\pm^{0.12}_{0.08}$	0.84 ± 0.14	2.94	$0.80\pm^{0.14}_{0.09}$
Fe-K line EW (eV)	305 ± 50	$470\pm^{200}_{75}$	405 ± 70	1600	$1080\pm^{100}_{180}$
Intensity (erg cm^{-2} s^{-1})	8.0×10^{-10}	6.6×10^{-10}	6.0×10^{-10}	2.6×10^{-10}	6.4×10^{-11}
χ^2/dof	104.2/89	94.2/89	131.9/89	383/83	85.6/84

Table 2. Partial covering fit results to the S3 and S4 spectra. The energies of the narrow Fe-L lines were fixed at the best-fit ASCA values in Mihara & Soong (1994). f is the fraction of the flux that undergoes extra absorption, N_{PCF}

Parameter	Spectrum	
	S3	S4
α	$0.864\pm^{0.02}_{0.04}$	0.74 ± 0.04
Blackbody kT (keV)	$0.083\pm^{0.006}_{0.002}$	0.089 ± 0.015
Equiv. BB radius (km)	$146\pm^{32}_{17}$	$145\pm^{11}_{21}$
N_H ($\times 10^{19}$ atom cm^{-2})	$2.0\pm^{4.1}_{2.0}$	11.0 ± 3.5
f	$0.723\pm^{0.023}_{0.013}$	0.35 ± 0.03
N_{PCF} ($\times 10^{22}$ atom cm^{-2})	6.03 ± 0.45	$21\pm^{12}_{6}$
Fe-L 0.91 keV EW (eV)	<35	<36
Fe-L 1.06 keV EW (eV)	<40	80 ± 45
Fe-K line energy (keV)	6.54 ± 0.10	6.56 ± 0.13
Fe-K line FWHM (keV)	1.59 ± 0.27	0.76 ± 0.23
Fe-K line EW (eV)	590 ± 80	$900\pm^{80}_{130}$
χ^2/dof	115.7/82	78.9/82

that this model adequately describes the M1, S1, S2 and S4 spectra, but not the S3 spectrum where a χ^2 of 383 for 83 degrees of freedom (dof) is obtained. The fit quality of the S2 spectrum is somewhat worse than to the M1, S1, and S4 spectra. This may be because of unresolved variability which was not excluded from the accumulation (see the upper and middle panels of Fig. 2). The S4 spectrum is significantly harder and the equivalent width (EW) of the Fe-K line is higher than the other spectra (Table 1). There is no comparable change in the EW of the Fe-L lines. The intense Fe-K feature is clearly visible in the S4 spectrum shown in Fig. 3. There is no significant change in Fe-K line energy between the spectra. The equivalent blackbody radii are $\sim$200 km for intervals M1, S1 and S2, decreasing to $\sim$150 km during S3 and $\sim$70 km during S4. The ratio of 0.1–10.0 keV flux in the blackbody component compared to the powerlaw is 16% for all the spectra except S3, where is it 9%.

The effects of significant absorption are clearly seen in the S3 spectrum as a change in spectral shape and increased curvature in the 1–3 keV range (see Fig. 3). This implies an absorption of $\gtrsim 10^{22}$ atom cm^{-2}. However, substantial flux remains $\lesssim$0.5 keV, which should be *completely* absorbed with such a high absorption. There are a number of possible explanations for such behavior: (1) the presence of separate "scattered" and "absorbed" spectral components, (2) partial covering of the emitting region(s), and (3) absorption by partially ionized material such that the low Z materials responsible for the majority of the absorption $\lesssim$0.5 keV are significantly ionized, while the higher Z elements are not. Possibilities (1) and (2) cannot be spectrally distinguished and are referred to as "partial covering", although this should be taken to include the possibility of separate scattering and absorbing regions. Partial covering can be modeled using the `pcfabs` model in XSPEC. Here a fraction, f, of the emission undergoes extra absorption, N_{PCF}, while the rest is absorbed by a low value of N_H, as before. The partial covering model gives an acceptable fit to the S3 spectrum (a χ^2 of 115.7 for 82 dof), while that of an ionized absorber (the `absori` model in XSPEC) is somewhat worse ($\chi^2 = 133.9$ for 83 dof). We therefore do not pursue further the ionized absorber fits since the partial covering model provides a better fit.

As previously stated, the "standard model" gives a significantly harder spectrum ($\alpha = 0.50 \pm 0.03$) for interval S4 than for the other spectra, where the average is $\sim$0.8. We have investigated whether this apparent hardness may result from a large amount of intrinsic absorption which, if not modeled correctly,

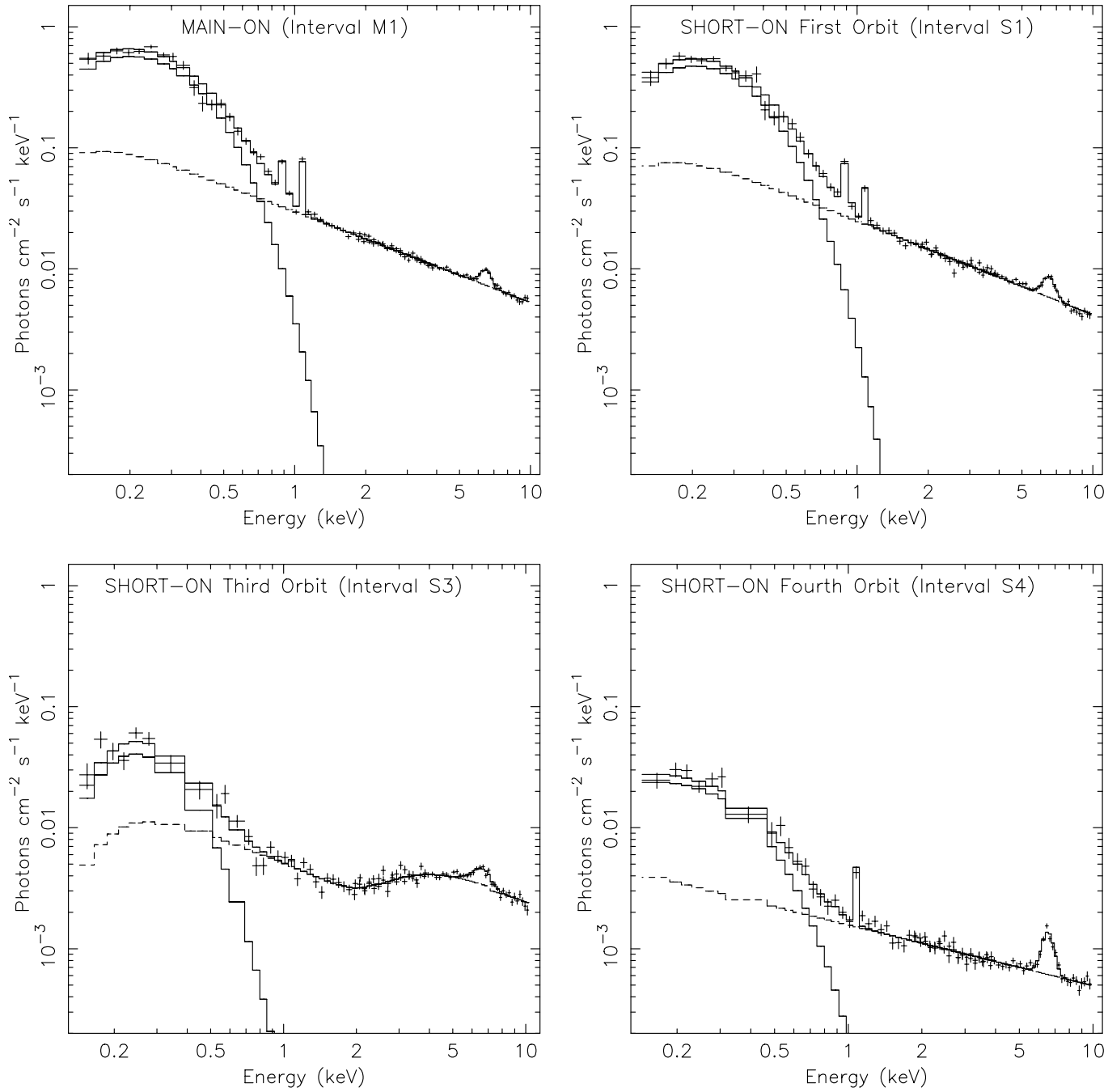

Fig. 3. LECS and MECS Her X-1 spectra during the main-on (M1) and short-on states (S1, S3, and S4). The solid lines show the unfolded spectrum obtained with the "standard" spectral model (see Table 1), while for S3 a partially covering absorber is used (see Table 2). The contributions from the blackbody and power-law components are indicated separately. The same scales have been used for all four panels. The effect of the large amount of absorption required in the S3 spectral fits is clearly seen as a change in the spectral slope around 2 keV

results in an anomalously hard spectral slope determination. The partial covering model was also fit to the S4 spectrum, even though the "standard" model provides an adequate description of the spectrum ($\chi^2 = 85.6$ for 84 dof). This gives a partial covering fraction of 0.35 ± 0.03 and extra absorption, $\mathrm{N_{PCF}}$, of $(2.1\pm^{1.2}_{0.6}) \times 10^{23}$ atom cm^{-2}. The best-fit value of α is now 0.74 ± 0.04, much closer to the values obtained in the other fits. This suggests that an explanation for the hard spectra (relative to the peak of the main-on state where $\alpha \sim 0.9$) seen at times from Her X-1 is the effects of large amounts of unresolved absorption, together with partial covering.

3.3. Pulse period and profile

The Her X-1 pulse periods were determined using only the non-dip and non-eclipse data obtained during the main- and short-on

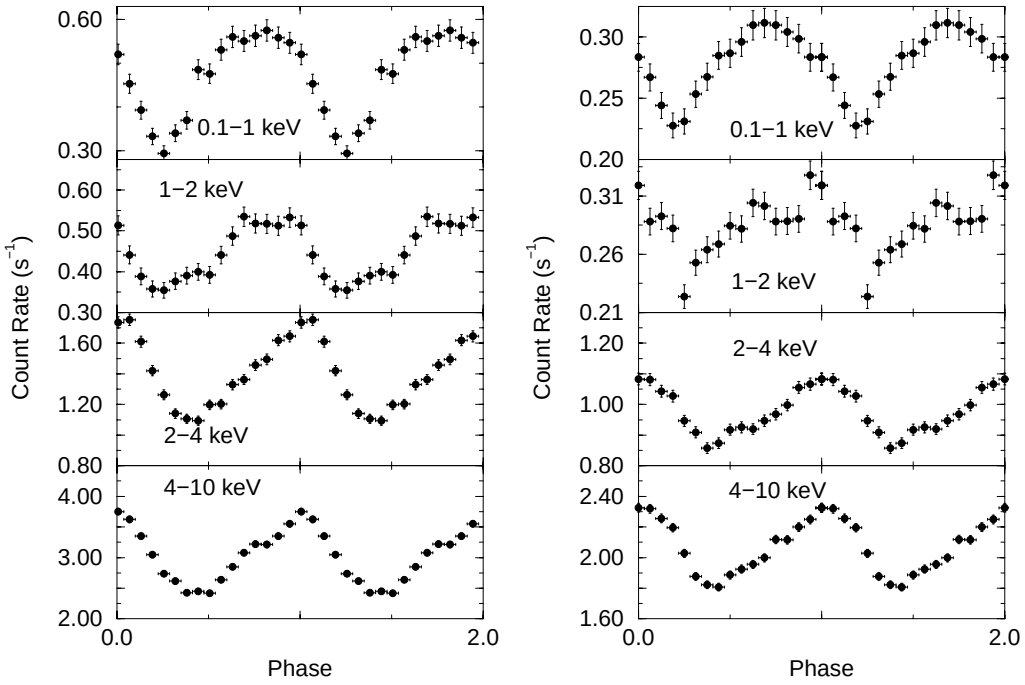

Fig. 4. Pulse profiles in 4 energy bands for the main- (left) and short-on (right) state observations. The 0.1–1 keV and 1–2 keV profiles are from the LECS and the 2–4 keV and 4–10 keV profiles from the MECS. Pulse phase 0.0 is defined as the maximum of the 4–10 keV folded lightcurves. The profiles are repeated for clarity

state observations. First, the arrival times of the photons were corrected to the solar system barycenter. Then the arrival times were additionally corrected to the Her X-1 center of mass using the ephemeris of Deeter et al. (1991). The periods were obtained with an epoch-folding technique using the MECS data, while the (1σ) uncertainties were determined by fitting the arrival times of sets of 6 averaged profiles. During the main- and short-on states the best-fit periods are 1.2377268 ± 0.0000009 s and 1.2377272 ± 0.00000015 s, respectively.

The pulse profiles obtained by folding the data with these best-fit periods in different energy bands are shown in Fig. 4. The well-known, strongly energy-dependent, pulse profile of Her X-1 is evident. In general, the main-on state profiles all exhibit greater modulation depth than those obtained during the short-on state. The smooth almost sinusoidal 0.1–1.0 keV profiles are dominated by emission from the blackbody and Fe-L lines, while the 2–4 keV and 4–10 keV profiles are dominated by the power-law. The 2–4 keV main-on state profile is more sharply peaked and has a larger amplitude than that obtained during the short-on state. The 1–2 keV energy range clearly marks the transition between the profiles dominated by these different spectral components and it has a very structured appearance. In this energy range the difference in profiles is the largest between the two on-states.

3.4. Pulse phase resolved spectrum

The data obtained during intervals S1 and S2 (short-on) and M1 were used to investigate the pulse phase dependence of the spectrum. Only the S1 and S2 intervals were included in the low-state accumulation since the spectra obtained during S3 and S4 are clearly different from those obtained elsewhere in the low-state. Both sets of data were divided into 10 equal phase bins, which gives comparable (within a factor of two) statistics. (Note that this is half the number of phase bins used by O97, since the total number of counts in both observations is much smaller than that in the SVP observation.) The spectra were rebinned and energy selected as above. The 10 phase-resolved spectra were fit using the "standard model" except that N_H, the Fe-L line energies, the Fe-K line energy and width and LECS/MECS relative normalization were fixed at their best-fit values obtained from the fits to the phase-averaged spectra (Table 1). The best-fit values from the M1 and S1 fits were used for the main- and short-on states phase resolved fits, respectively.

The fits to the phase-resolved spectra give acceptable values of χ^2_ν of typically 0.9–1.3 for 80–110 dof. Fig. 5 shows the variations in best-fit spectral parameters as a function of pulse phase. Variations in all the fit parameters, except the strengths of both Fe lines and the blackbody kT are evident. Comparison of the left- and right-hand panels of Fig. 5 shows that the phase differences between the blackbody and power-law normalizations are approximately the same for the main- and short-on states. The amplitude of variation of the power-law component is smaller during the short-on state observation ($\sim$25%), compared to during the main-on state observation ($\sim 50\%$). The intensity of the Fe-L line appears to be relatively constant. The phase dependence of the Fe-K line intensity is not well determined, but is consistent with having the same behavior as the power-law normalization, or with having no variation with pulse phase. This is in contrast to the *Ginga* results of Choi et al. (1994), where the blackbody and Fe-K line normalizations appear to be correlated.

The ratio of the blackbody to power-law fluxes are, during the main-on state, 18% and 15% for the pulse minima and maxima, respectively and 16% and 20% during the short-on state. Similar values can be derived from O97. This means that the reprocessing fraction is similar in all the observations, imply-

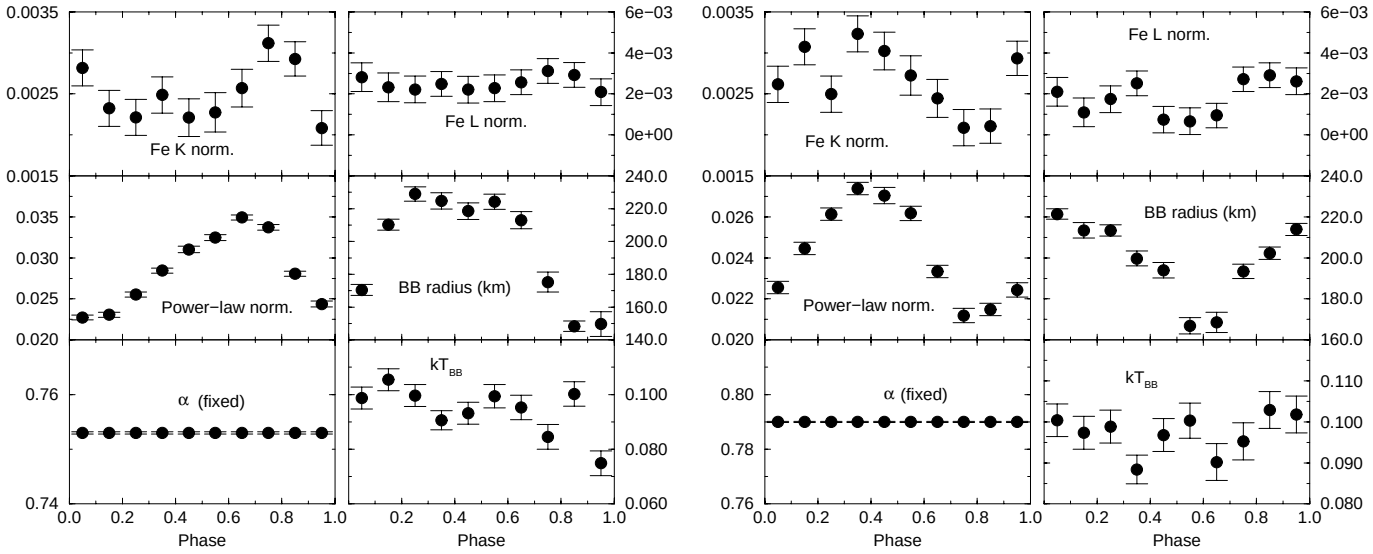

Fig. 5. Best-fit spectral parameters as a function of pulse phase for the main- (left) and short-on (right) state observations. The units of normalization are: for the power-law: Photons at 1 keV, cm^{-2} keV^{-1} s^{-1}, for the Gaussian features: Photons cm^{-2} s^{-1}, and for the blackbody: $\mathrm{L}_{39}/\mathrm{d}_{10}^2$, where L_{39} is the source luminosity in 10^{39} erg s^{-1} and d_{10}^2 is the source distance in units of 10 kpc. Note that the power-law index, α, was kept constant. Uncertainties denote the 68% confidence interval for 1 parameter of interest ($\Delta\chi^2 = 1.0$). Phases are arbitrary, but identical for each observation

ing that the amount of reprocessing does not depend strongly on Φ_{35}. The best-fit equivalent blackbody radii are consistent with being identical between the main-on and the beginning (S1 and S2) of the short-on at $\sim$210 km, while in the latter phases of the short-on it decreases to $<$100 km. This may indicate that about 75% the blackbody reprocessing site is obscured during the later parts of the short-on state.

A cross-correlation between the best-fit power-law and blackbody normalizations obtained during the main- and short-on states reveals that in both cases the phase difference is consistent with a separation of $250 \pm 20°$. This value is marginally consistent with the phase difference of $215 \pm 20°$ obtained earlier in the main-on state by O97. However, due to the broad, asymmetric profiles that are different in each observation (see Fig 5 and O97) it is difficult to reliably measure the pulse phase difference between the two components and so probe any changes of (relative) positions of the emission and reprocessing regions.

4. Discussion

We report on a long (5.7 day duration) observation of most of the short-on state of Her X-1 with the BeppoSAX LECS and MECS together with a short observation during the declining phase of the preceding main-on state. We find that the main-on and early short-on state spectra can be well fit with the standard blackbody and power-law continuum model, together with Fe-L and Fe-K emission features. During the later phases of the short-on there is evidence for intervals of strong low-energy absorption. These intervals repeat each 1.7 day orbital cycle, becoming increasingly long and occurring earlier in each orbital cycle as the short-on state progresses. This behavior appears to be consistent with the predictions of the warped disk model of e.g., Schandl & Meyer (1994) and Schandl (1996) where the end of the short-on state is caused by the accretion disk moving into the line of sight to the neutron star. These results therefore support the idea that the Her X-1 system contains a warped, precessing, accretion disk.

The shape and intensity of the S4 spectrum is very similar to that measured by Mihara et al. (1991) during the *low-state* of Her X-1 by *Ginga*. They model the spectrum with "scattered" and absorbed ($\mathrm{N_H}$= 10^{24} atom cm^{-2}) components and a power-law index equivalent to that found in the main-on state. In addition, their best-fit Fe-K line energy, FWHM and EW of 6.53 ± 0.08 keV, 0.8 ± 0.4 keV, and 1.0 ± 0.1 keV, respectively are all strikingly similar to those reported here for interval S4 (Table 1). These BeppoSAX observations therefore support the idea, first proposed by Mihara et al. (1991), that the low-state Her X-1 emission contains at least two components, one of which is significantly absorbed.

The pulse profiles (broad and almost sinusoidal) in both the main- and short-on states are consistent with those reported by Deeter at al. (1998) obtained with *Ginga* at similar Φ_{35}. Deeter et al. (1998) show that the pulse shape during the main-on state changes rapidly from a clearly peaked shape to a much broader, more sinusoidal, shape during the final stages of the main-on state. The best-fit pulse periods demonstrate that Her X-1 is continuing its recent spin-up trend as shown in Bildsten et al. (1997).

The pulse phase difference of the maxima of the power-law and blackbody during the short- and main-on state observations is consistent with being the same, and consistent with the results of O97, obtained earlier in the main-on state. Such a symmetry is expected for a reprocessing region located at, or near, the inner edge of the accretion disk since at $\Phi_{35} = 0.0$ and 0.5 the same behavior is predicted. This is because of the symmetrical

disk shape expected unless the region of the disk where the reprocessing occurs is strongly warped (see e.g. Heemskerk & van Paradijs 1989 for this "symmetry-rule"). This somewhat strengthens the association of the blackbody component with reprocessed emission originating from the inner edge of the accretion disk. Ideally, it would be preferable to track the phase difference between the components over the entire 35 day cycle. However Her X-1 is only visible as a strong X-ray source for two intervals separated by about half the 35 day cycle, giving rise to a similar phase dependence of the components. This, combined with the large pulse profile changes, make it difficult to reliably restrict the location of the reprocessing site.

Acknowledgements. The BeppoSAX satellite is a joint Italian and Dutch programme. T. Oosterbroek acknowledges an ESA Research Fellowship. The quick-look RXTE ASM data were provided by the ASM/RXTE team. We thank the staff of the BeppoSAX Science Data Center for assistance with these observations.

References

Anders E., Grevesse N., 1989, Geochim. Cosmochim. Acta 53, 197
Becker R.H., Boldt E.A., Holt S.S., et al., 1977, ApJ 214, 879
Bildsten L., Chakrabarty D., Chiu J., et al., 1997, ApJS 113, 367
Boella G., Chiappetti L., Conti G., et al., 1997, A&AS 122, 327
Catura R.C., Acton L.W., 1975, ApJ 202, L5
Choi C.S., Nagase F., Makino F., et al., 1994, ApJ 437, 449
Choi C.S., Seon K.I., Dotani T., Nagase F., 1997, ApJ 476, 81
Crosa L., Boynton P.E., 1980, ApJ 235, 999
Deeter J.E., Boynton P.E., Miyamoto S., et al., 1991, ApJ 383, 324
Deeter J.E., Scott D.M., Boynton P.E., et al., 1998, ApJ 502, 802
Gerend D., Boynton P.E., 1976, ApJ 209, 562
Giacconi R., Gursky H., Kellog E., et al., 1973, ApJ 184, 227
Heemskerk M.H.M., van Paradijs J., 1989, A&A 223, 154
Jones C., Forman W., 1976, ApJ 209, L131
Mavromatakis F., 1993, A&A 273, 147
McCray R.A., Shull J.M., Boynton P.E., et al., 1982, ApJ 262, 301
Mihara T., Soong Y., 1994, In: Makino F. (ed.) Proc. of New Horizon of X-ray astronomy. Universal Academy, Tokyo, p. 419
Mihara T., Makishima K., Ohashi T., Sakao T., Tashiro M., 1990, Nat 346, 250
Mihara T., Ohasi T., Makishima K., et al., 1991, PASJ 43, 501
Morisson D., McCammon D., 1983, ApJ 270, 119
Oosterbroek T., Parmar A.N., Martin D.D.E., Lammers U., 1997, A&A 327, 215 (O97)
Parmar A.N., Sanford P.W., Fabian A.C., 1980, MNRAS 192, 311
Parmar A.N., Martin D.D.E., Bavdaz M., et al., 1997, A&AS 122, 309
Petterson J.A., 1977, ApJ 218, 783
Pravdo S.H., Becker R.H., Boldt E.A., et al., 1977, ApJ 215, L61
Reynolds A.P., Parmar A.N., 1995, A&A 297, 747
Reynolds A.P., Quiantrell H., Still M.D., et al., 1997, MNRAS 288, 43
Schandl S., 1996, A&A 307, 95
Schandl S., Meyer F., 1994, A&A 289, 149
Scott D.M., Leahy D.A., 1999, ApJ 510, 974
Shulman S., Friedman H., Fritz G., Henry R.C., Yentis D.J., 1975, ApJ 199, L101
Tananbaum H., Gursky H., Kellog E.M., et al., 1972, ApJ 174, L143
Trümper J., Pietsch W., Reppin C., et al., 1978, ApJ 219, L105
Vrtilek S.D., Mihara T., Primini F.A., et al., 1994, ApJ 436, L9